System Identification of a Radio-Frequency Ion Thruster

IEPC-2015-292／ISTS-2015-b-292

Presented at Joint Conference of 30th International Symposium on Space Technology and Science,
34th International Electric Propulsion Conference and 6th Nano-satellite Symposium
Hyogo-Kobe, Japan
July 4–10, 2015

Niklas Wolf* and Uwe Probst†
University of Applied Sciences, Giessen, 35390, Germany

and

Peter J. Klar‡
University of Giessen, Giessen, 35392, Germany

Abstract: In this work, we present an analysis of a radio-frequency ion thruster (RIT) regarding its static and dynamic behavior. The investigations will be used for the design of a control system referred to as beam current controller (BCC). For the automized recording of measured data, the RIT and its peripherals like the high voltage power supplies (NHV, PHV), the power supply (DC power) of the radio-frequency generator (RFG), and the mass flow controller (MFC) were implemented into a real-time measurement unit. Additionally, the measurement of the grid currentsand the beam current as a result are implemented. This gives us the opportunity to control and measure the relevant input and output data of the RIT and to determine the behavior of the beam current as a function of different input parameters of the peripherals described above.

The static behavior: e.g., the beam current as a function of the grid voltages or the DC input power to the RFG as a function of the mass flow at constant beam current, can be obtained and will be used to define different working points of the RIT. The dynamic behavior is examined by varying one input parameter while keeping all other parameters constant and then investigating the influence of the former on the beam current. The data is then used for system identification; i.e., a mathematical description of the dynamic behavior in the investigated point of operation.

The real-time measurement unit is explained and the measurements of the static and dynamic behavior are presented. At the end the mathematical description of one working point is determined and simulated for two different types of input parameters.

*Research Assistant, Department of Electrical Engineering, niklas.wolf@ei.thm.de
†Professor, Department of Electrical Engineering, uwe.probst@ei.thm.de
‡Professor, Institute of Experimental Physics I, peter.j.klar@exp1.physik.uni-giessen.de

Nomenclature

RIT	= radio-frequency ion thruster
BCC	= beam current controller
NHV	= negative high voltage
PHV	= positive high voltage
MFC	= mass flow controller
RFG	= radio-frequency generator
I_{scr}	= current from screen grid to ground
I_{acc}	= current from accelerator grid to ground
I_{gnd}	= current from ground grid to ground
I_{beam}; I_{b}	= ion beam
V_{scr}	= positive voltage at screen grid
V_{dec}	= negative voltage at acceleration grid
V_{gnd}	= satellite ground
V_{acc}	= voltage between screen and acceleration grid
m_{i}	= mass of singly ionized particles
$\dot{m}$	= mass flow of propellant (xenon)
P_{rfg}	= DC-power to the radio-frequency generator
F	= thrust
$RTMU$	= real-time measurement unit
$\mathbf{e}$	= error vector
$\mathbf{\Psi}$	= data matrix
$\mathbf{\Theta}$	= real parameter vector
$\widehat{\mathbf{\Theta}}$	= estimated parameter vector
$\mathbf{W}$	= instrumental variable matrix
N	= number of data points
$\mathbf{y}$	= output vector

I. Introduction

Electric propulsion is a technology aimed at achieving thrust with high exhaust velocities and thereby decreasing the amount of propellant required for a given space mission or application compared to other conventional (chemical) propulsion methods.Requiring less propellant reduces the launch mass leading to lower costs. Electric propulsion in general encompasses propulsion technology where electricity is used to increase the propellant exhaust velocity, e.g., arcjet technology, Hall thrusters, ion thrusters, resistojets, and other types of electric thrusters.

Together with University of Giessen our research group works on optimizing the radio-frequency ion thrusters' overall efficiency by developing models describing the RF thrusters' impedance and performance[5] and electromagnetic interference (EMI)[6] as well as the development of a radio-frequency generator[7]. Ion thrusters exhibit the highest efficiency and very high specific impulse compared to other thruster types. However, a major fallback of ion thrusters is the erosion of the grids as a result of inefficient ion optics and a so called "over-pervance". The erosion of the grids limits the lifetime of a RIT. Consequently, it is important to minimize erosion of the grids to maximize lifetime.

An additional part of the investigation is the performance mapping which relates DC power consumption of the RFG to the massflow of the gas (propellant). It is necessary to minimize the required propellant consumption with respect to the required power which the system has to provide and the heat the system has to handle.

The beam current controllers role is to control the beam current considering the optimal operating point with regard to the rf-power, the massflow, and the ion optics.

II. RIT Operation Pinciple

Thrust generation in RITs can be divided into two steps. Before thrust is generated at the ion accelerator, where the static electric field accelerates electrically charged propellant particles, it is necessary to ionize the propellant. Figure 1 shows the schematic of a RIT.

A neutral noble gas, commonly Xenon, is used as the propellant due to high atomic mass. The gaseous flow into the ionizer is controlled and limited by the MFC. The ionizer chamber, a vessel made of an isolating material, is surrounded by a rf-coil. A signal in the range of some megacycles is coupled into the coil and induces an axial magnetic field. As a result, the primary magnetic field induces a secondary electric field which accelerates free electrons to gain energy for impact ionization. With any ionizing impact of an electron and a neutral xenon particle, an additional electron/ion pair is created. Once the ionization process is triggered, a self-sustaining plasma-discharge takes place.

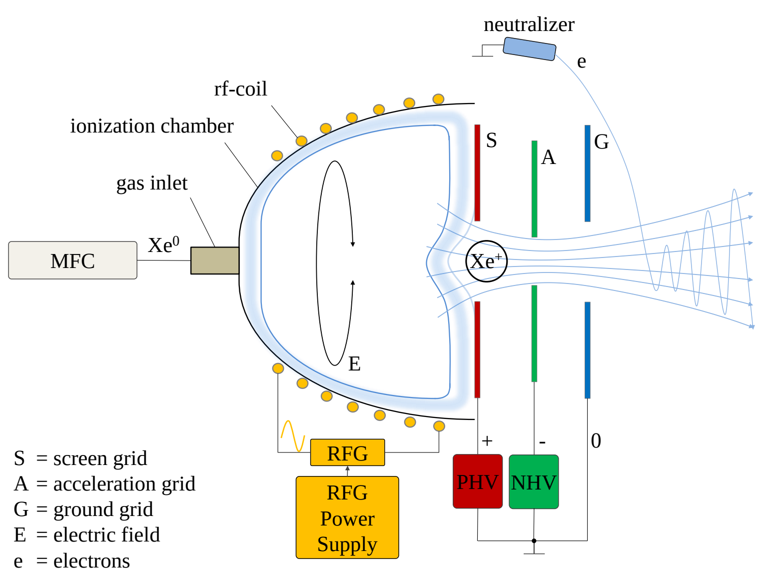

Figure 1. Function principle of a RIT.

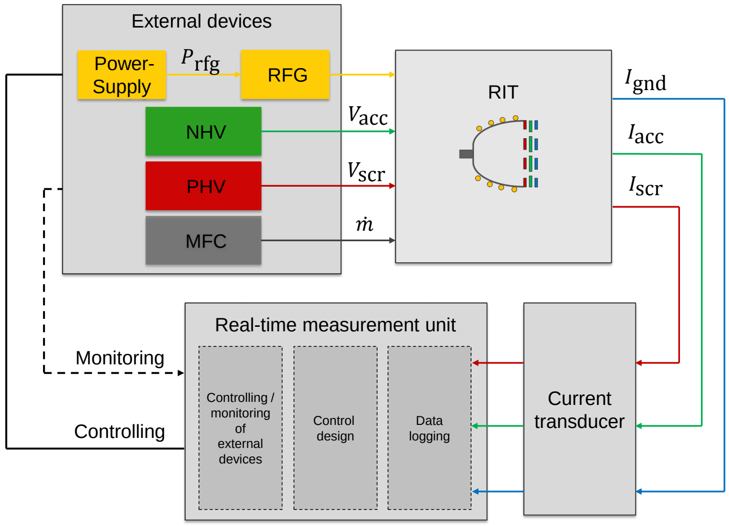

Figure 2. Schematic of the test setup for measurements at the RIT.

After ionization, thrust can be generated by applying a positive voltage at the grid facing the plasma, the screen grid, and a negative voltage at the following acceleration grid. This second grid is used to prevent backstreaming of electrons from the surroundings into the chamber. It also allows one to employ a higher voltage for ion extraction ($V_{\rm scr} + |V_{\rm dec}|$). A third grid, the ground grid on satellite ground, protects the thruster from surrounding ions to hit the acceleration grid.

The neutralizer, positioned outside the thruster, provides electrons to neutralize the generated ion beam and to maintain the potential of the thruster and spacecraft relative to the space plasma potential.[8]

III. Test Setup

For measuring data and testing new control systems, the RIT and its periphals were integrated into a real-time measurement unit (RTMU). As shown in Fig. 2 the grid currents $I_{\rm scr}$, $I_{\rm acc}$, $I_{\rm gnd}$ are recorded via current transducer digitalized via analog-digital converter inside the RTMU. The periphals - RFG power supply, NHV, PHV, and MFC - are also monitored by A/D-converters and controlled by D/A-converters. The system offers extra outputs like RS232 and other digital ports.

Matlab and Simulink serve as the system's software basis which enables automized data measurement and acquisition while controlling the different parameters in real-time.

IV. Static and Dynamic Behavior of the RIT

As mentioned earlier, thrust is generated at the ion accelerator, the grid-system outside the ionization chamber. Disregarding the atomic contribution given by atoms which leave the RIT with thermal velocity, the thrust can be defined as follows:[1,3]

$$F = I_{\rm b}(V_{\rm acc}, P_{\rm rfg}, \dot{m})\sqrt{\frac{2m_{\rm i}V_{\rm scr}}{e}} \tag{1}$$

As Eq. (1) shows, thrust is dependant on the beam current $I_{\rm beam}$, the atomic mass of the ions, the elementary charge, and the screen voltage $V_{\rm scr}$ at the "inner grid". The beam current, with only singly ionized particles taken into account, depends on the power fed into the rf-coil (DC power, $P_{\rm rfg}$), the mass flow of xenon ($\dot{m}$), and the acceleration voltage given by the total voltage between screen grid and acceleration grid, disregarding the potential of the plasma:

$$V_{\rm acc} = V_{\rm scr} + |V_{\rm dec}| \tag{2}$$

In summary, thrust can be controlled by the four different input parameters

a) Positive high voltage at the screen grid - V_{scr}

b) Negative high voltage at the acceleration grid - V_{dec}

c) Mass flow - $\dot{m}$

d) DC-power to the RFG - P_{rfg}

which will be investigated in the following sections with respect to the beam current given by:

$$I_{\mathrm{beam}} = |I_{\mathrm{scr}}| - I_{\mathrm{acc}} - I_{\mathrm{gnd}} \tag{3}$$

The operating point of interest in this work is defined as a beam current in the range of 5 mA.

A. Static Characteristics

1. Beam current versus grid voltages

As mentioned before, it is necessary to minimize the currents at the acceleration and ground grid due to erosion which may occur inevitably due to inefficient ion optics. The currents arise from electrons flowing to the grids to recombine with impacting ions. Figure 3 shows the currents as a function of the voltage at the screen grid for different negative voltages V_{dec}.

$|I_{\mathrm{scr}}|$ increases with rising screen voltage as expected. The current I_{gnd} decreases with the voltage at the screen grid and generally diminishes with increasing V_{acc} defined in Eq. (2). I_{acc}, the leakage current at the second grid, depends on the deceleration voltage while all curves are increasing for a screen voltage greater 500 V. The beam current as a result of all three currents increases with $V_{\mathrm{scr}}^{3/2}$ while getting limited by the sheath thickness of the plasma at higher grid voltages.[3]

The optimal operating range lies between a screen voltage of 275 V (at $V_{\mathrm{dec}} = -250$ V) to 750 V (at $V_{\mathrm{dec}} = -50$ V).

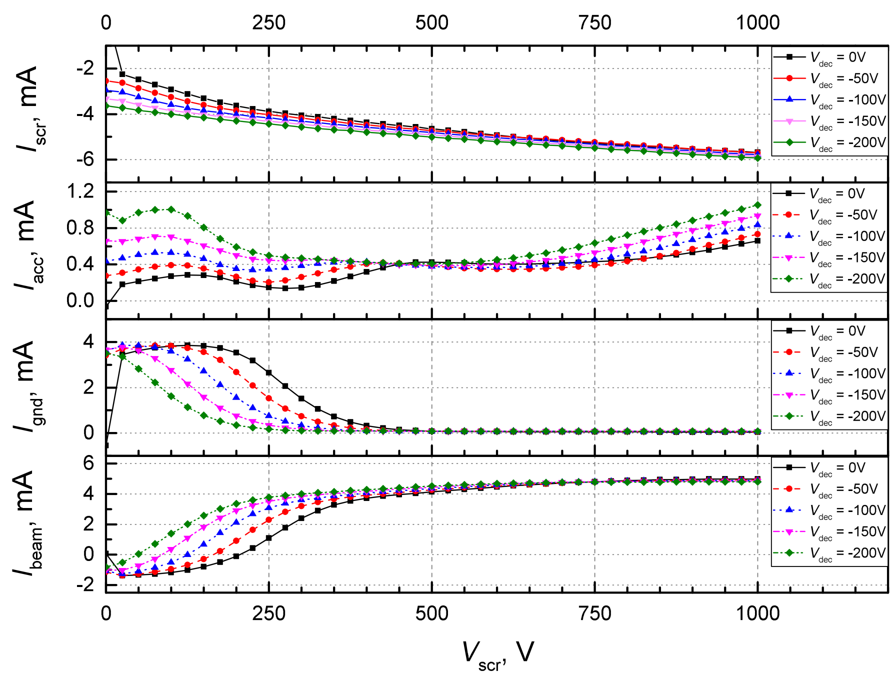

Figure 3. Measured static behavior of the beam current as a function of the grid voltages at a xenon mass flow of 0.45 sccm and a RFG DC input power of 22.5 W.

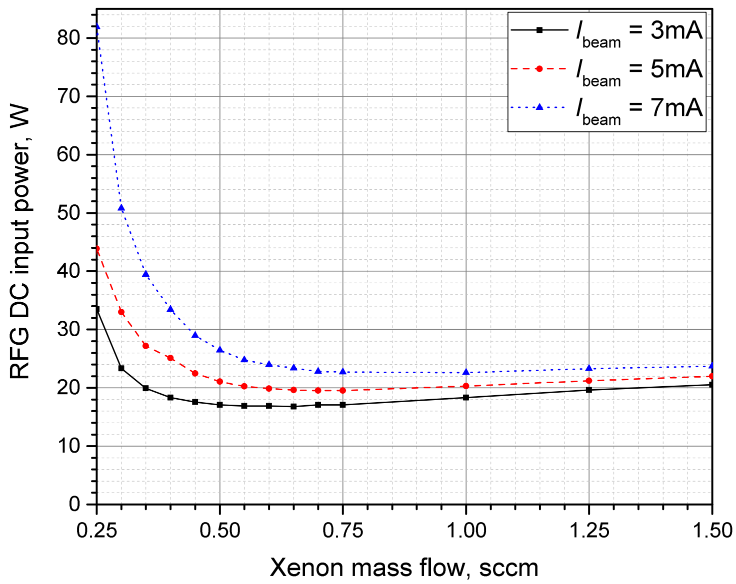

Figure 4. Determined performance mappings of three different beam currents at $\mathbf{V}_{scr} = \mathbf{1000}$ V and $\mathbf{V}_{scr} = \mathbf{-150}$ V.

2. RFG DC input power versus mass flow

As a typical characteristic curve, the performance mapping connects the DC power forwarded into the RFG with mass flow at fixed beam current. The optimal operating point depends on the requirements of the particular mission. For low mass flow, a higher DC input power is required and higher mass flow for lower DC rf power limits the lifetime with respect to the propellant used. It follows that a minimum mass flow and a DC rf power as low as possible are necessary for an optimal operating point. Figure 4 shows the relation and the curves at $I_{\text{beam}} = 3$ mA, 5 mA, and 7 mA.

For the investigation of the dynamic behavior the operating point was defined at $\dot{m} = 0.453$ sccm and $P_{\text{rfg}} \approx 23$ W $- 25$ W.

B. Dynamic Characteristics

To design a controller, knowledge about the system's dynamic behavior is required. For this reason, the input data mass flow and the RFG DC input power were changed in small steps around the operating point.

First, the influence of the DC rf power on the beam current was measured, as demonstrated in Fig. 5. The figure shows the constant mass flow and the changing beam current with respect to the changing DC power. It seems that the current instantly follows the change of the input without any delay.

Figure 6 shows the beam current depending on the change of the mass flow. Unlike in previous observations, the changing mass flow also affects the second input, the DC power. Due to changing mass flow, the plasma changes inside the chamber which affects the electrical load of the RFG. While the DC voltage is held constant, the DC current and, as a consequence, the DC power decreases too. These relations have to be considered in the following steps of model design and system identification.

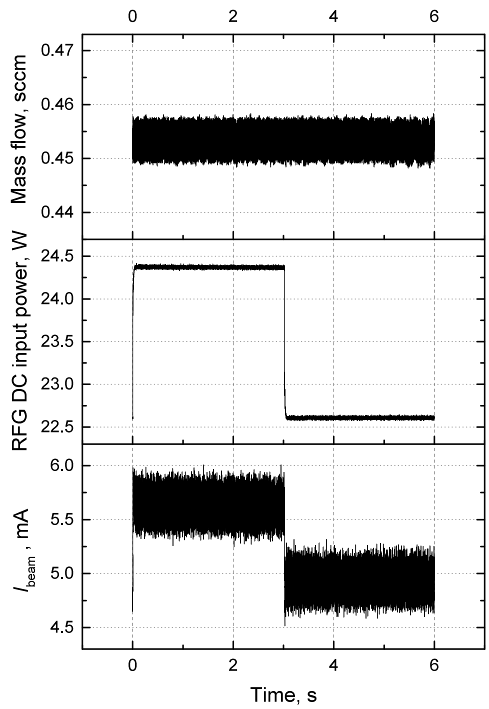

Figure 5. Modification of the beam current by changing the rf-power. Operating point at $\mathbf{P}_{\text{rfg}} = \mathbf{23.4}$ W $\pm\,\mathbf{0.9}$ W, $\dot{\mathbf{m}} = \mathbf{0.453}$ sccm.

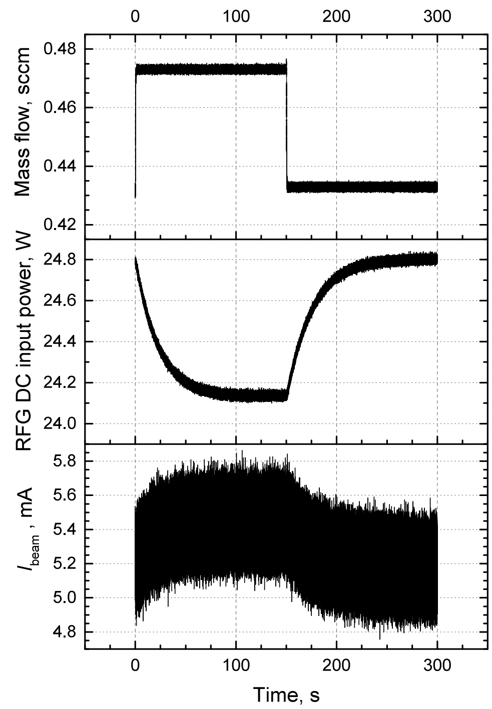

Figure 6. Modification of the beam current by changing the mass flow. Operating point at $\mathbf{P}_{\text{rfg}} = \mathbf{24.8}$ W, $\dot{\mathbf{m}} = \mathbf{0.453}$ sccm $\pm\,\mathbf{0.02}$ sccm

V. System Identification

System identification approaches are used to obtain mathematical descriptions of physical systems. In this context, the description, or mathematical model, ought to describe the systems dynamic behavior as simply as possible and as detailed as necessary. The physical dependencies of the system are thus shown in a transfer function, seen in Eq. (4):

$$G(s) = \frac{b_{n-1} \cdot s^{n-1} + b_{n-2} \cdot s^{n-2} + ... + b_1 \cdot s^1 + b_0}{s^n + a_{n-1} \cdot s^{n-1} + a_{n-2} \cdot s^{n-2} + ... + a_1 \cdot s^1 + a_0} \tag{4}$$

The transfer function describes the behavior between output and input signal, omitting inner physical processes.

A. Instrumental Variables Method (IV)

The Instrumental Variables Method (IV) is a method of evaluating the system's behavior which avoid the problem of biased estimates which occur when using the method of least squares.[5] IV uses the implementation of an auxiliary variable and is based on the model equation of the equation error:

$$\mathbf{e} = \mathbf{y} - \mathbf{\Psi\Theta} \tag{5}$$

Multiplying both sides with the transpose of the auxiliary variable, the instrumental variable matrix $\mathbf{W}$, yields:

$$\mathbf{W}^T\mathbf{e} = \mathbf{W}^T\mathbf{y} - \mathbf{W}^T\mathbf{\Psi\Theta} \tag{6}$$

If the instrumental variables; i.e., the elements of $\mathbf{W}$, are chosen such that

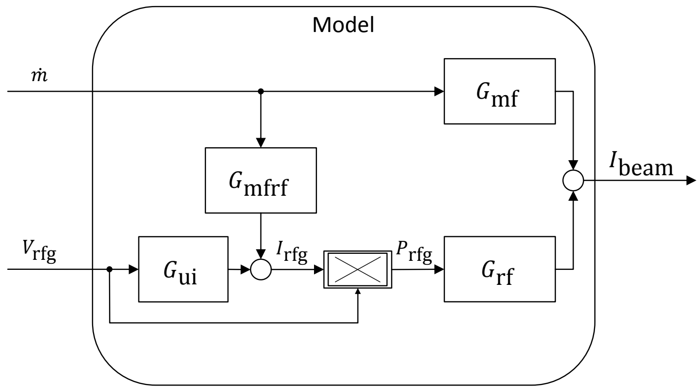

Figure 7. Block diagram of the expected simulation model.

$$p \lim_{N\to\infty} \mathbf{W}^T \mathbf{e} = \mathbf{0} \tag{7}$$

and

$$p \lim_{N\to\infty} \mathbf{W}^T \mathbf{e} = \mathbf{0} \text{ positive definite,} \tag{8}$$

it follows from Eq. (6):

$$p \lim_{N\to\infty} \mathbf{W}^T \mathbf{\Psi}\mathbf{\Theta} = p \lim_{N\to\infty} \mathbf{W}^T \mathbf{y} \tag{9}$$

The estimation equation is then given by:

$$\widehat{\mathbf{\Theta}} = (\mathbf{W}^T \mathbf{\Psi})^{-1} \mathbf{W}^T \mathbf{y} \tag{10}$$

The structure and definitions of the matrices are given in Ref. 2 in more detail.

B. Simulations

As mentioned earlier, the influence of the mass flow on the second input, the DC current, has to be considered within the model and the identification. Figure 7 shows the expected model with the identified transfer functions in Tab. 1.

For the simulations the measured inputs ($\dot{m}$, I_{rfg}, V_{rfg}) were applied to the model. The resulting outputs are demonstrated in Fig. 8 (I_{beam}) and Fig. 9 (I_{beam} and I_{rfg}) as the flattened lighter curve inside the measured input and output data (black).

Table 1. Identified transfer functions.

Input	Output	Short term	Transfer function
RFG DC input voltage	RFG DC input current	G_{ui}	$\frac{87.123\cdot 10^{-3}}{1+s\cdot 5.388\cdot 10^{-3}}$
RFG DC input power	Beam current	G_{rf}	$3.976\cdot\frac{1+s\cdot 1.402\cdot 10^{-3}}{1+s\cdot 9.810\cdot 10^{-3}+s^2\cdot 4.627\cdot 10^{-6}}$
Mass flow	RFG DC input current	G_{mfrf}	$\frac{-1.271}{1+s\cdot 24.155}$
Mass flow	Beam current	G_{mf}	$\frac{13.411}{1+s\cdot 25.189}$

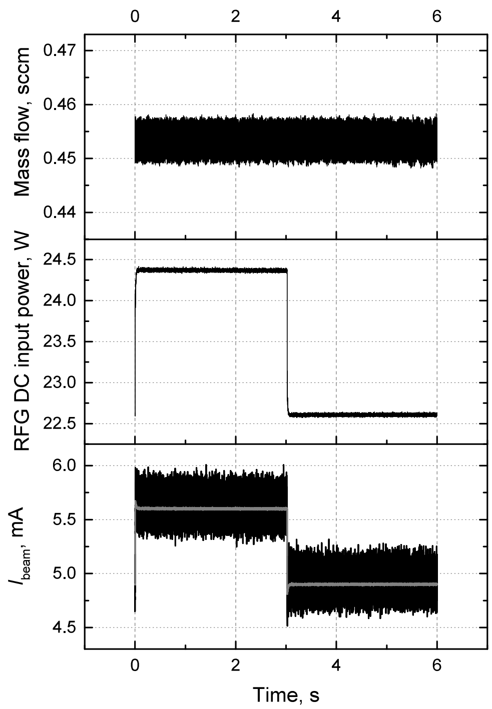

Figure 8. Simulation of the dynamic behavior of the beam current versus the RF-power.

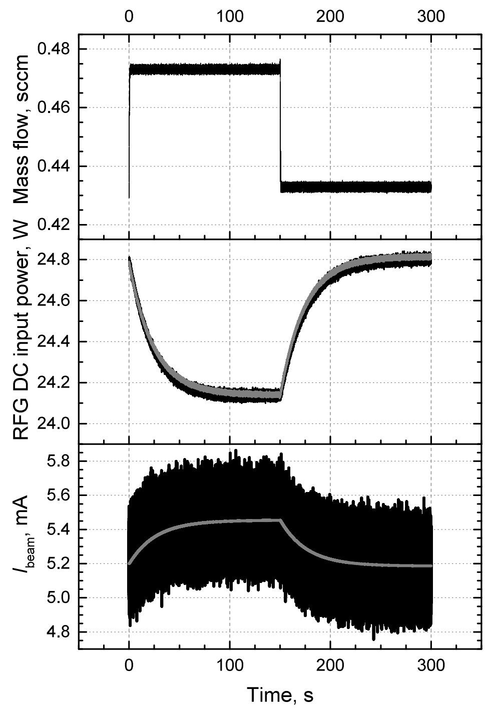

Figure 9. Simulation of the dynamic behavior of the beam current versus the massflow.

VI. Conclusion and Outlook

In this paper, we presented the investigation of the system's static and dynamic behavior and the identification of two input parameters in one operating point. For this purpose a real-time measurement unit was established to control and monitor the peripherals as well as to measure the grids' current. It was shown that the method of instrumental variables is suitable for the identification for this particular operating point and that the simulated systems behavior matches the data experimentally obtained.

As mentioned above, the mass flow influences the load of the RFG because it changes the plasma inside the chamber. The model described in Ref. 5 may be used to prove this dependence.

The identified transfer functions of the systems dynamic behavior will be tested for additional working points, in terms of mass flow and DC rf power, for different beam currents. The identification has to be iteratively performed until the models match for different working points. Also, the influence of the change of the grid voltages needs to be investigated.

Control systems will be included for the identified points of operation and examined for robustness and behavior. To be able to account for the erosion of the grids a recursive identification (or online identification) and an adaptive control system would be desirable in the future.

References

[1]Goebel, D. M., and Katz, I., *Fundamentals of Electric Propulsion*, John Wiley & Sons, Hoboken, 2008, Chap. 2.

[2]Isermann, R., and Muenchhof, M., *Identification of Dynamic Systems*, Springer-Verlag, Berlin, 2011, Chaps. 8-10.

[3]Freisinger, J., Loeb, H. W., and Scharmann, A., "Radiofrequency ion beam source RIM-10 for material processing," Kerntechnik 51, 1987, pp. 125-128.

[4]Koehler, P., "Design und Inbetriebnahme eines Strahlprofil-Detektors und azimutale Strahlanalyse an Triebwerken des μN RIT-Typs," Diploma-Thesis, University of Giessen, Giessen, 2010.

[5]Volkmar, C., Ricklefs, U., and Klar, P. J., "Self-Consistent Numerical 1D/3D Hybrid Modeling of Radio-Frequency Ion Thrusters", Proceedings of the 34th International Electric Propulsion Conference, ERPS, USA, 2015.

[6]Baruth, T., and Thüringer, R., "Radiated Emission Simulation of a RIT4", Proceedings of the 34th International Electric Propulsion Conference, ERPS, USA, 2015.

[7]Simon, J., Probst, U., and Klar, P. J., "Development of a Radio-Frequency Generator for RF Ion Thrusters", Proceedings of the 34th International Electric Propulsion Conference, ERPS, USA, 2015.

[8]Leiter, H. J., Killinger, R., Bassner, H., Müller, J., Kukies, R., and Fröhlich, T, "Development and performance of the advanced radio frequency ion thruster RIT-XT", Proceedings of the 28th International Electric Propulsion Conference, ERPS, USA, 2003.